TEKTONIKA

Investigating Global Correlations Between Earthquake-generated Tsunamis and Subduction Zone Characteristics

Iris van Zelst [*1,2,3], **Silvia Brizzi** [4], **Elenora van Rijsingen** [4,5,6,7], **Francesca Funiciello** [4], **Ylona van Dinther** [1,7]

[1]Seismology and Wave Physics, Institute of Geophysics, Department of Earth Sciences, ETH Zürich, Zürich, Switzerland | [2]Institute of Planetary Research, German Aerospace Center (DLR), Berlin, Germany | [3]Now at: School of GeoSciences, University of Edinburgh, Edinburgh, UK | [4]Laboratory of Experimental Tectonics, Dip. Scienze, Roma Tre University, Rome, Italy | [5]Laboratoire de Géologie, École Normale Supérieure, PSL Research University, CNRS-UMR 8538, Paris, France | [6]Géosciences Montpellier, CNRS, Montpellier University, Montpellier, France | [7]Department of Earth Sciences, Utrecht University, Utrecht, The Netherlands

Abstract Tsunamigenic earthquakes pose a large hazard in subduction zones, but it is currently unclear in which - if any - tectonic setting they preferentially occur. Here, we compile the global Subduction Nature & Interconnected Tsunamigenic earthquake Characteristics (SNITCH) database with parameters on subduction geometry, tectonics, and megathrust seismicity, and 329 tsunami events caused by earthquakes that were recorded in subduction zones between 1962 and 2018. We aim to identify potential correlations between tsunamigenic earthquake behaviour and subduction zone characteristics. We first use a bivariate regression analysis to find first-order correlations between the normalised number of earthquake-generated tsunami events N_t and the megathrust seismicity and tectonic parameters characterising a subduction zone. We confirm self-evident correlations between N_t and the number and magnitude of earthquakes and subduction kinematics. We then apply a multivariate Fisher analysis to see which combination of tectonic parameters best distinguishes subduction zone segments in which relatively many and few tsunami events caused by earthquakes have occurred. Despite the scarcity of the tsunami data, we consistently find that the type of margin (i.e., erosional or accretionary), the trench-normal component of the subduction and convergence velocity, the amount of trench sediments, and the roughness of the incoming plate are related to the number of earthquake-generated tsunami events. Our results therefore suggest that tsunamigenic earthquakes may occur more frequently in tectonic settings where plates subduct relatively fast beneath a sediment-starved, erosional margin with a complex, shallow subduction interface, characterised by multiple faults and fractures.

Executive Editor:
Craig Magee
Associate Editor:
Jack Williams
Technical Editor:
Mohamed Gouiza

Reviewers:
Jonathan Griffin
Qiang Qiu

Submitted:
19 July 2024
Accepted:
20 February 2025
Published:
17 March 2025

Tsunamigenic earthquakes are defined as earthquakes that cause tsunamis and usually occur on thrust faults in subduction zones. In the past decades, tsunamigenic earthquakes have greatly impacted society, with the most notable events being the 2004 M_w 9.1–9.3 Sumatra-Andaman earthquake and resulting Indian Ocean tsunami, and the 2011 M_w 9.0 Tōhoku-Oki earthquake and tsunami (e.g., *Lay et al.*, 2005; *Titov et al.*, 2005; *Fujii et al.*, 2011; *Ozawa et al.*, 2011). During these large events, the megathrust typically plays the most important role, as it provides the largest potential slip area, and is therefore capable of producing the largest earthquake with an accompanying tsunami. However, other faults than the megathrust, such as normal faults in the outer rise or splay faults in the imbricate thrust system in the subduction wedge, likely play an important role in tsunamigenesis as well (e.g., *Fukao*, 1979; *Sibuet et al.*, 2007; *Waldhauser et al.*, 2012; *Hubbard et al.*, 2015; *von Huene et al.*, 2016; *Fan et al.*, 2017; *Sladen and Trevisan*, 2018). Since these faults have steeper dips than the megathrust, they can accommodate more vertical displacements for similar amounts of slip (*Wendt et al.*, 2009; *Hananto et al.*, 2020; *Van Zelst et al.*, 2022). However, it is difficult to determine whether an earthquake ruptured along the megathrust or a splay fault, due to the uncertainty in earthquake and tsunami source localisation (*Sibuet et al.*, 2007; *Waldhauser et al.*, 2012).

The large megathrust earthquakes responsible for generating the largest tsunami events are typically associated with a smooth incoming plate and a large trench sediment thickness (*Ruff*, 1989; *Heuret et al.*, 2012; *Wang and Bilek*, 2014; *Scholl et al.*, 2015; *Brizzi et al.*, 2018; *Van Rijsingen et al.*, 2018). Similarly, a buried megathrust (*Carvajal et al.*, 2022), slip depth (*Carvajal et al.*, 2022), structural features on the incoming plate, such as subducting fracture zones and

*✉ iris.vanzelst@ed.ac.uk

fault structures (*Robinson et al.*, 2006; *Jiang et al.*, 2022) and ridges, (*Gahalaut et al.*, 2010), and megathrust geometry and dip (*Oryan and Buck*, 2020; *Jiang et al.*, 2022) have been suggested as factors influencing the rupture, velocity, and tsunamigenic potential of earthquakes in subduction zones.

Tsunami earthquakes are a subset of tsunamigenic earthquakes (*Satake and Tanioka*, 1999; *Satake*, 2015) defined by their disproportionally large tsunami waves compared to their seismic waves (*Kanamori*, 1972a). They are typically associated with sediment-starved, erosional margins, because these settings can sustain very shallow slip due to their shallow frictional regime (*Polet and Kanamori*, 2000; *Bilek*, 2010; *Geersen*, 2019; *Meng and Duan*, 2023). In contrast, it has also been suggested that sediment-rich margins with at least a thin layer of subducting sediment could promote several aspects typical for 'slow tsunami earthquakes' — a subset of tsunami earthquakes. The lower rigidity and strength of sediments could for example facilitate their slow rupture velocities (*Polet and Kanamori*, 2000). Similarly, the sudden uplift of sediments in the accretionary wedge along high-angle splay faults, which is typically larger in accretionary margins with large amounts of trench sediments, during an earthquake could account for large vertical displacements of the water column (*Seno*, 2002; *Tanioka and Seno*, 2001; *Van Zelst et al.*, 2022).

Additionally, there is evidence that tsunami earthquakes tend to occur in regions with rough incoming plates (*Tanioka et al.*, 1997; *Polet and Kanamori*, 2000; *Bell et al.*, 2014; *Geersen*, 2019; *Wang and Lin*, 2022), where the degree of roughness of an incoming plate is defined by the size and distribution of topographic features, such as seamounts, horst and graben structures, and ridges. For example, the 1947 Offshore Poverty Bay and Tolaga Bay earthquakes in New Zealand have been suggested to stem from rupture over a subducted seamount (*Bell et al.*, 2014).

Hence, the observed relationship between large ($M_w >$ 8.5) megathrust earthquakes, the amount of trench sediments in a subduction zone, and incoming plate roughness appears to be contrary to the relationship observed for tsunami earthquakes. However, it is unclear how tsunamigenic earthquakes, which include both large megathrust earthquakes and tsunami earthquakes, are affected by trench sediments and incoming plate roughness. Indeed, a global assessment, including statistics on the relationship between tsunamigenic earthquakes and general subduction zone characteristics, is still missing.

Here, we aim to contribute to the ongoing debate of factors behind earthquake-related tsunami hazard by providing insights into broad patterns of earthquake tsunamigenesis. To this end, we combine a subduction zone characteristics and megathrust seismicity database with a tsunami database. We investigate the relationships between earthquake-generated tsunamis, megathrust seismicity, and the tectonic setting of subduction zones. Using bi- and multivariate statistical analyses, we identify subduction zone characteristics associated with the occurrence of tsunamigenic earthquakes.

1 The SNITCH database

We compile a database containing parameters on megathrust seismicity, seismogenic zone geometry, subduction zone tectonics, and tsunami events caused by earthquakes in 62 subduction segments. We call this database the Subduction Nature & Interconnected Tsunamigenic earthquake Characteristics (SNITCH) database. The SNITCH database is compiled from two main sources. First, we use the subduction zone database containing data on subduction zone characteristics and megathrust seismicity presented in *Heuret et al.* (2011, 2012); *Brizzi et al.* (2018) and *Lallemand et al.* (2018). Secondly, we extract tsunami events caused by earthquakes from the NOAA NGDC/WDS Global Historical Tsunami database (*Global Historical Tsunami Database*, Retrieved: February 1, 2019). In the following, we describe how we assemble the entire database in detail.

1.1 Subduction zone characteristics

We use the subduction zone characteristics from the database of *Heuret et al.* (2011), and its subsequent versions (*Heuret et al.*, 2012; *Brizzi et al.*, 2018). This database consists of 62 subduction zone segments (Figure 1) derived from merging 505 subduction zone transects based on homogeneous megathrust seismicity, homogeneous seismogenic zone geometry, or rupture areas for $M_w \geq 8.0$ earthquakes confined in a single segment. Available subduction zone parameters in this database include for example the number of earthquakes that has occurred in a subduction zone segment, as well as information on the cumulative seismic moment and largest magnitude a subduction zone has seen, parameters describing the geometry of the megathrust and seismogenic zone, and parameters on the velocity and age of the subducting plate (see Table 1).

In addition to these parameters, we include two parameters that quantify the roughness of the seafloor of the incoming plate prior to subduction according to *Lallemand et al.* (2018): long (i.e., 80–100 km) and short (i.e., 12–20 km) wavelength roughness. These parameters serve as a proxy for the roughness on the subduction interface (*Lallemand et al.*, 2018). The different wavelengths are sensitive to different styles of topographic features on the subducting plate. Short wavelength roughness is typically associated with small- and intermediate-sized seamounts. Long wavelength roughness typically relates to large seamounts, seamount chains, and oceanic ridges. To translate the data provided by *Lallemand et al.* (2018) to the format of the 62 subduction zone segments used here, we average the roughness values for all transects comprising one subduction segment. This results in a total of 25 different parameters that quantify the subduction nature and seismicity of the 62 subduction segments (Table 1).

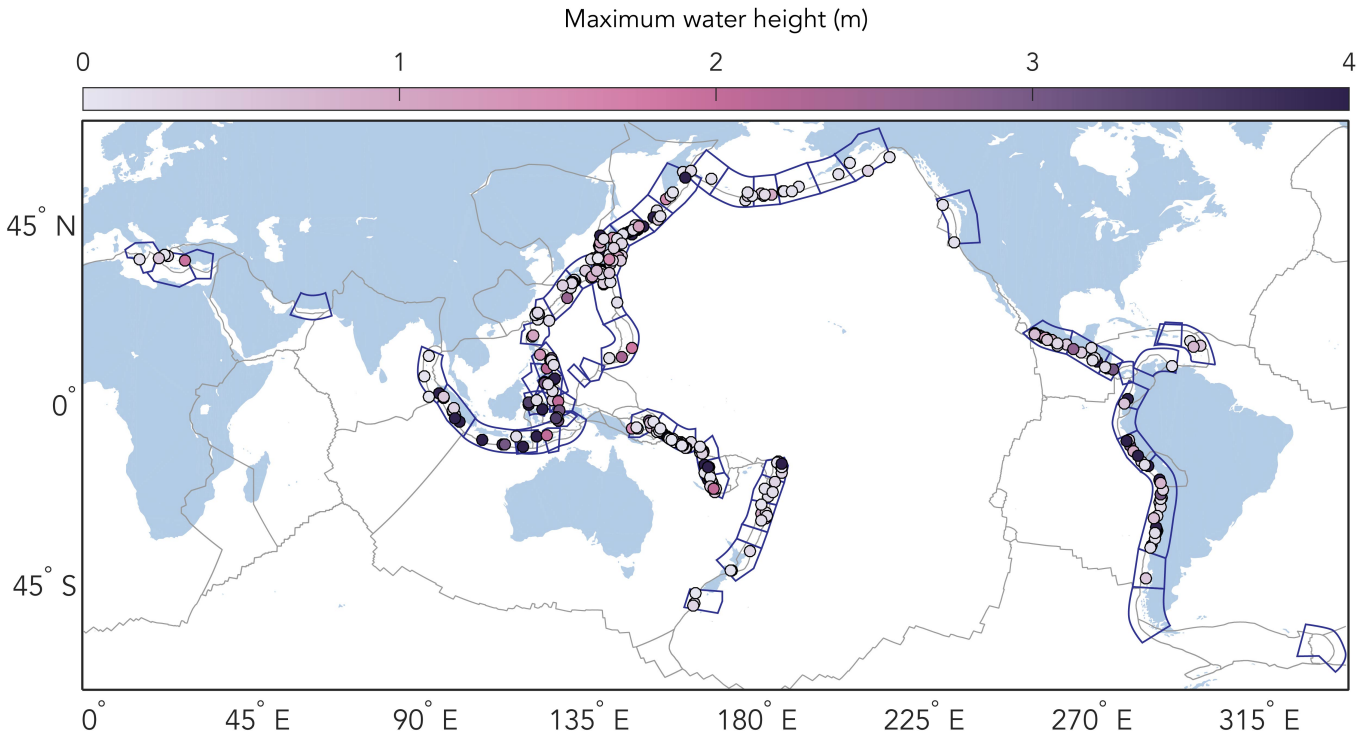

Figure 1 – All 329 definite tsunami events caused by an earthquake in the NOAA NGDC/WDS Global Historical Tsunami Database that occurred from 1962 to 2018, organised into the subduction zone segments (dark blue) defined by *Heuret et al.* (2011). To illustrate the size of the tsunami events, they are coloured by maximum observed water height above sea level extracted from the NOAA NGDC/WDS Global Historical Tsunami Database. This includes two types of measurements: (1) a tide gauge measurement where the maximum tsunami height is defined as half of the maximum height (minus the normal tide) of a tsunami wave recorded at the coast by a tide gauge; and (2) the run-up height, which is defined as the maximum elevation the wave reaches at the maximum inundation. Since these two measurements are conflated into one parameter in the NOAA NGDC/WDS Global Historical Tsunami Database, they are used in this work solely for illustrative purposes and have not been used in the statistical analysis.

We sort these parameters in three different categories to simplify the analysis: megathrust seismicity, geometric, and tectonic parameters. The megathrust seismicity parameters result from earthquake observations from the ISC-GEM Global Instrumental Earthquake (*Storchak et al.*, 2013) and Centennial-Harvard CMT catalogues spanning from 1900 to 2007 (see *Heuret et al.*, 2011; *Brizzi et al.*, 2018, for more details). The majority of the geometric parameters of the seismogenic zone (with the exception of $W_{\text{intraslab}}$) is derived from megathrust seismicity from 1900 to 2007 according to *Heuret et al.* (2011) (Figure 2). Therefore, these geometric parameters only shed light on the geometry of the seismogenic zone along the megathrust and do not include information on the geometry of the deeper slab, the overriding plate structure or other tectonic features such as splay or outer rise faults. To provide a first-order measure of slab geometry at depth in addition to seismogenic zone geometry, $W_{\text{intraslab}}$ represents the downdip length of the slab. This parameter is estimated from the distribution of intraslab earthquakes recorded in the area, expanding the dataset used in *Heuret et al.* (2011) beyond megathrust earthquakes (*Brizzi et al.*, 2018). The tectonic parameters are independent of any earthquake catalogue, and give insight into the nature of the subducting and overriding plate, the large scale geometry of the system, such as the distance between the volcanic arc and the trench $D_{\text{arc-trench}}$, and the kinematics of the subduction zone.

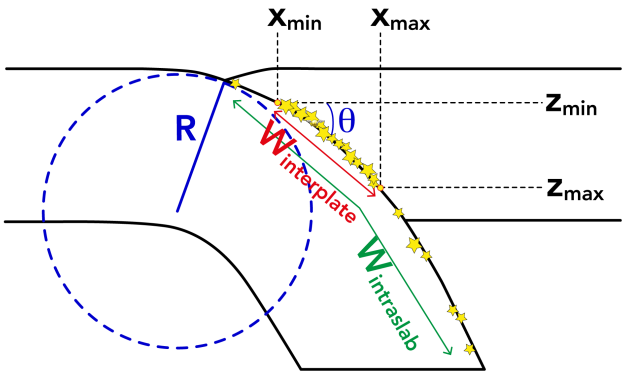

Figure 2 – Diagram based on *Heuret et al.* (2011) showing how the geometric parameters in the SNITCH database are estimated based on the extent of megathrust seismicity (yellow stars). Abbreviations for parameters are explained in Table 1.

Table 1 – Parameters in the SNITCH database

Symbol	Parameter	Unit
	Megathrust seismicity parameters	
N_{eq}	Number of subduction plate interface thrust earthquakes from 1976 to 2007 with $M_w \geq 5.5$ and from 1900 to 1975 with $M_w \geq 7.0$	-
τ	Seismicity rate: number of events per century and per 10^3 km trench	-
CSM	Cumulative seismic moment	N m
M_{mrr}	Equivalent representative magnitude in the sense of *Ruff and Kanamori* (1980)	-
$M_{\text{max,GEM1900}}$	Maximum M_w from 1900–2007 according to the ISC-GEM catalogue	-
$M_{\text{max,Cent\&CMT}}$	Maximum M_w from 1900–2007 according to the Centennial & CMT catalogues	-
$M_{\text{max,GEM1960}}$	Maximum M_w from 1960–2007 according to the ISC-GEM catalogue	-
	Geometric parameters (based on seismicity)	
z_{min}	Depth of the updip limit of the seismogenic zone	km
z_{max}	Depth of the downdip limit of the seismogenic zone	km
x_{min}	Distance from the trench to the updip limit of the seismogenic zone	km
x_{max}	Distance from the trench to the downdip limit of the seismogenic zone	km
$W_{\text{interplate}}$	Downdip width of the seismogenic zone	km
θ	Dip of the megathrust	°
R	Curvature radius of the slab at the trench	km
$W_{\text{intraslab}}$	Downdip length of the slab	km
	Tectonic parameters	
L^*	Trench-parallel extent of the subduction zone segment	km
A	Age of the subducting plate at the trench	Myr
$D_{\text{arc-trench}}$	Mean distance between the volcanic arc and the trench	km
UPS	Upper plate strain *1 = extension (E); 2 = neutral (N); 3 = compression (C)*	-
T_{sed}	Sediment thickness at the trench	km
$AvsE$	Type of margin *0 = accretionary (A); 1 = erosional (E)*	-
R_{sw}	Short wavelength roughness (12-20 km)	m
R_{lw}	Long wavelength roughness (80-100 km)	m
v_{sn}	Trench-normal component of the subduction velocity from *DeMets et al.* (1990)	mm year^{-1}
v_{cn}	Trench-normal component of the convergence velocity from *DeMets et al.* (1990)	mm year^{-1}
	Tsunami event parameters	
N_t	Normalised number of tsunami events per km trench	-
$N_{t,\text{tot}}$	Total number of tsunami events in a subduction zone segment	-

1.2 Earthquake-generated tsunami events

We download data from the NOAA NGDC/WDS Global Historical Tsunami Database (*Global Historical Tsunami Database*, Retrieved: February 1, 2019) as the NOAA database is well suited for studying the statistics on the occurrence of tsunamis (*Gusiakov et al.*, 2019). We select definite tsunami events that were caused by an earthquake from 1962–2018. We choose 1962 to start our data retrieval, because of the instalment of the World-Wide Standardised Seismograph Network that year, which ensured global monitoring of earthquakes. Prior to 1962, the NOAA NGDC/WDS Global Historical Tsunami Database is potentially incomplete which could skew our statistical analysis. Using the 1962–2018 time window, we extract 395 earthquake-generated tsunami events. Note that due to this limited time window, large historical tsunamigenic earthquakes such as the 1944 M_w 8.0-8.3 Tonankai (*Kanamori*, 1972b), 1945 M_w 8.2 Makran (e.g., *Heidarzadeh and Satake*, 2015), 1946 M_w 8.1-8.4 Nankaido (*Kanamori*, 1972b), 1946 M_w 7.4 Aleutian (*López and Okal*, 2006), and 1960

M_w 9.4-9.6 Chile (*Kanamori and Cipar*, 1974; *Satake and Atwater*, 2007) earthquakes are not included in the SNITCH database. Because some of the subduction parameters in the SNITCH database are based on megathrust seismicity data up to 2007 (Section 1.1), we make a second version of the SNITCH database with earthquake-generated tsunami events limited to 2007, which consists of 284 earthquake-generated tsunami events. Hence, there are two versions of the SNITCH database: SNITCH-2007 and SNITCH-2018. Note that large recent tsunamigenic earthquakes such as the 2010 M_w 8.8 Maule (*Delouis et al.*, 2010) and 2011 M_w 9.0 Tōhoku earthquakes (*Fujii et al.*, 2011) are not part of the SNITCH-2007 database due to the applied time window. As this narrower time frame further limits the already scarce tsunami data from the *Global Historical Tsunami Database* (Retrieved: February 1, 2019) we only use the SNITCH-2007 database for direct comparison with subduction zone parameters on megathrust seismicity in our bivariate analysis.

For each tsunami event caused by an earthquake in the NOAA NGDC/WDS Global Historical Tsunami Database, we extract its tsunami source location (i.e., the earthquake epicentre). We sort all the tsunami events caused by earthquakes into the subduction zone segments defined by *Heuret et al.* (2011) based on their tsunami source location. For the SNITCH-2018 database, 66 events are situated outside the subduction zone segments. For example, the 2018 Palu-Koro earthquake and tsunami falls outside the Sulawesi subduction zone segment. This is because this event is a rare nearby strike-slip induced tsunami and hence not associated with any subduction system. We remove all these events from our analysis, as they are not associated with tsunamigenic earthquakes in subduction zones. This results in a total of 329 tsunami events caused by earthquakes (or tsunamigenic earthquakes) in the SNITCH-2018 database (Figure 1). In the SNITCH-2007 database, 47 tsunami events are situated outside the subduction zone segments, so the final SNITCH-2007 database consists of 237 tsunami events caused by earthquakes.

As the subduction zone segments consist of rectangular transects, they can overlap in some places. If a tsunami is placed in an area where two or more subduction zone segments overlap, we manually assign it to a segment. For this purpose, we consider the depth of the earthquake, which better suggests with which subducting plate, and hence which subduction zone segment, a tsunami event should be associated. Hence, we assign the tsunami event to a subduction zone segment based on tomographic studies and mapped slabs from e.g., SLAB1.0 (*Hayes et al.*, 2012). In total, there are 46 tsunamis (14% of all tsunami events in SNITCH-2018) that are manually sorted into subduction zone segments according to their depth and the subduction geometry at depth. Note that there are no tsunami events associated with ruptures that span multiple segments, as the subduction zone segments are defined such that they encapsulate the largest rupture width that occurred in that region (*Heuret et al.*, 2011).

Considering the limited amount of data in the SNITCH database due to the short observational time window, it is useful to consider a scale-free measure of tsunamigenesis for our statistical analyses. To this end, we count the amount of earthquake-generated tsunami events in each subduction zone ($N_{t,\mathrm{tot}}$) and calculate the normalised number of tsunami events per km trench N_t

$$N_t = \frac{N_{t,\mathrm{tot}}/L^*}{\max(\mathrm{N_{t,tot}}/\mathrm{L^*})},$$

where L^* is the along-strike length of a subduction segment. Scaling with L^* ensures that the only parameters distinguishing the different subduction zone segments are physical parameters. This includes the number of earthquakes, which would logically correlate with the number of earthquake-generated tsunami events (as we demonstrate in Section 2.2). However, since the relationship between the number of earthquakes in a subduction zone and its physical parameters (including subduction velocity) is not completely straightforward, we refrain from further complicating our N_t measure of tsunami events and biasing our analysis towards certain parameters.

As such, N_t is a normalised measure of earthquake tsunamigenesis independent of the size of the subduction segments. We therefore deem N_t the most reliable quantity to gain any insights into the relationship between tectonics and tsunamigenesis and we focus our analysis on N_t.

The Japan subduction segment has the highest number of normalised tsunami events per km trench, resulting in $N_t = 1$. After Japan, the South Kuril subduction segment has the highest N_t of 0.77, followed by the Bougainville ($N_t = 0.49$; part of the Solomon Islands archipelago), and Nankai ($N_t = 0.47$) subduction segments. The normalised number of tsunami events per km trench is also high in the rest of the Nankai-Ryukyu subduction zone, with the Southern Ryukyu and Northern Ryukyu subduction segments sporting values of N_t of 0.30 and 0.19, respectively. Close to the Bougainville subduction zone segment, the New Hebrides also shows an overall large number of normalised tsunami events per km trench with $N_t = 0.39$ in the Southern Hebrides, $N_t = 0.44$ for the D'Entrecasteaux segment, and $N_t = 0.32$ for the Northern Hebrides subduction segment.

Subduction segments that have experienced large tsunamigenic earthquakes events in recent years, such as Andaman and Chile have a lower N_t of 0.06 and 0.21, respectively.

There are also a significant amount of subduction zone segments where no tsunami events have been recorded (i.e., $N_t = 0$) from 1962 – 2018, including the East Aegean, Makran, Palau, Northern Peru, Panama, Sandwich, and Southern Kermadec segments. Naturally, this raises the question whether the available observational record is sufficient for the type of statistical analysis we perform. We address this potential limitation of our approach in detail in Section 4.1.

Unfortunately, N_t is not a perfect parameter to quantify the tsunamigenic behaviour of subduction zones, although we believe no better parameter exists at present. For similar values of N_t, the detailed tsunami history of different regions can be vastly different as there is no distinction between, e.g., the tsunami magnitude. In the same vein, N_t does not take into account the maximum earthquake magnitude of a certain region, while it is generally assumed that larger earthquakes are more likely to produce tsunamis as they are in theory capable of producing larger surface displacements.

Ideally we would be able to use some sort of measure of tsunami energy per fault length for each subduction zone in our database. This is however impossible to quantify with the currently available tsunami data as the extent of the rupture on the faults that excited the tsunami is often uncertain and the effect of a tsunami is hard to quantify and depends largely on coastal factors. Finite fault models, such as those provided by *Hayes* (2017) and *Ye et al.* (2016), could offer more information on tsunami energy by incorporating rupture extent and seafloor deformation. However, these models typically only exists for megathrust earthquakes with relatively high magnitudes ($M_w \geq$ 7.0-7.5) and are limited to short time frames (e.g., from 1990 onwards compared to the 1962 – 2018 time frame of the SNITCH database). Given these limitations, our simple approximation of performing the analysis purely on the normalised number of tsunamis per subduction segment allows us to gain a first-order indication of the parameters that play a role in the physical mechanism of tsunamigenesis and the frequency or recurrence interval of tsunamis and tsunamigenic earthquakes. More importantly, although the lack of information on size and energy of the tsunamis in N_t could be perceived as a limitation of our method, it also allows us to approach the process of tsunamigenesis without any bias towards the size of the triggering earthquake event. As such, we can investigate whether there are any subduction zone parameters that are conducive to the physical process of generating a tsunami, regardless of the size of the tsunami that ensues.

2 Bivariate statistical analysis: a first-order look into relationships between tsunami events and subduction zone characteristics

2.1 Methods

We calculate the Pearson's product-moment correlation coefficient R_p between the number of tsunami events, N_t and $N_{t,\text{tot}}$, and the parameters quantifying different subduction zone characteristics (see *Van Zelst*, 2025, for the scripts used). The Pearson's product-moment correlation coefficient gives insight into the linear correlation between two variables. To reduce the effect of outliers on linear correlations, we also calculate the Spearman rank correlation coefficient ρ, in which the similarity or monotonicity between two variables is assessed, regardless of any linear relationship that might exist between them.

To focus our analysis, we consider a relationship between two variables worthy of further investigation if both the Pearson and Spearman correlations are higher than or equal to 0.3 (*Heuret et al.*, 2011) with p-values smaller than 0.05 (i.e., there is less than a 5% chance that the null hypothesis of there being no correlation is true). p-values for the Spearman correlations are indicated by p and p-values for Pearson correlations are indicated by p_p. For visualising our results, we show Spearman's rank correlation coefficient (Section 2.2), because it typically shows the highest correlations. This is due to the fact that the data is not linear, and can more easily be described by a monotonic relationship. However, the differences in correlation coefficients between the two methods is on average only a few percent. The results for Pearson's product-moment correlation coefficient can be found in the Supporting Information.

2.2 Results

The Spearman's rank correlation coefficient matrix of the tsunami event parameters of SNITCH-2007 and the megathrust seismicity parameters is shown in Figure 3a. N_t correlates well with the number of earthquakes N_{eq} (ρ = 0.57), the seismicity rate τ (ρ = 0.63), and the various measures of the maximum earthquake magnitude ($0.34 < \rho < 0.46$). This indicates that more tsunamis are associated with subduction zone segments that have experienced larger megathrust earthquakes.

There are no significant correlations between the geometric parameters describing the seismogenic zone and subducting plate and the occurrence of tsunami events of SNITCH-2007 (Figure 3b) in this bivariate analysis.

The tectonic parameters describe the large scale structure, geometry, kinematics, and nature of the subduction zone. Since the tectonic parameters are not influenced by a limited observational time span, we correlate them with the tsunami events from the SNITCH database including entries until 2018 (Figure 3c).

We find a positive correlation between the type of margin $AvsE$ and N_t (ρ = 0.35), which translates to erosional margins being associated more with tsunami events. This is corroborated by the negative correlation between N_t and T_{sed} (ρ = -0.40).

N_t also correlates positively with the trench-normal component of the subduction and convergence velocity (v_{sn} and v_{cn}; $\rho = 0.66$ and $\rho = 0.47$, respectively), which complies with the general idea that more tsunamigenic earthquakes would be recorded during the same time span in settings where the stress build-up is more rapid. However, as seen in the scatter plots in Figure 4, the relationships are not perfectly straightforward, although the trends are clearly visible. This is likely because other factors besides the velocity, such as the coupling on the interface, also play a first-order role in earthquake frequency.

Figure 4 further shows that large N_t only occurs for low sediment thickness T_{sed}, although there is

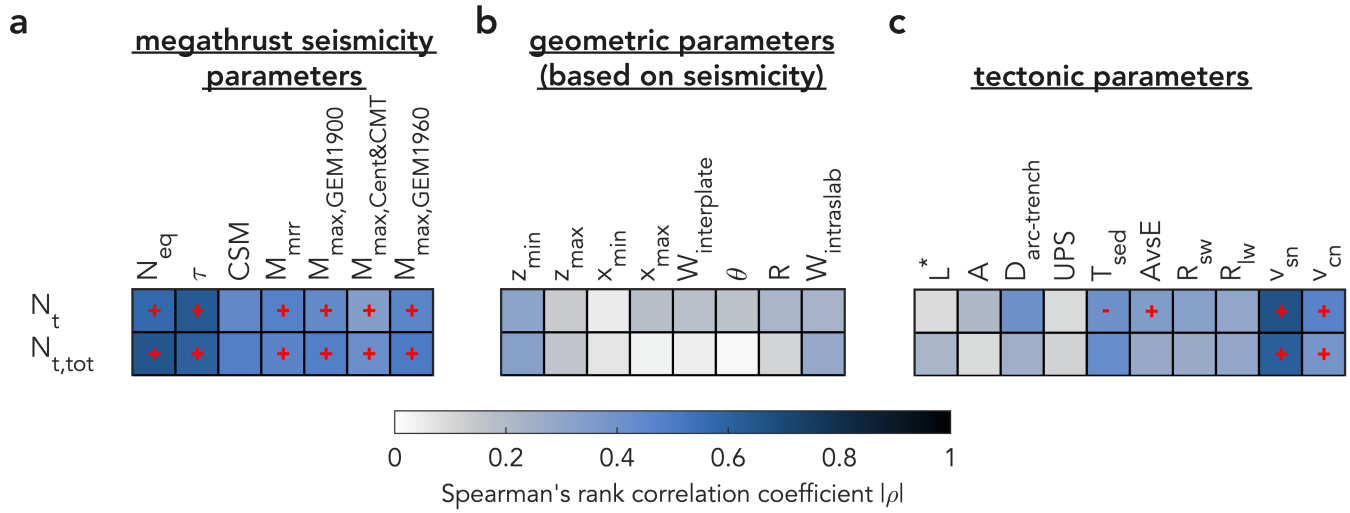

Figure 3 – Spearman's rank correlation coefficients of (a) the SNITCH-2007 tsunami event parameters correlated with the megathrust seismicity parameters; (b) the SNITCH-2007 tsunami event parameters correlated with the geometric parameters (based on seismicity); and (c) the SNITCH-2018 tsunami event parameters correlated with tectonic parameters. Significant positive and negative correlations worthy of further investigation as defined in Section 2.1 are indicated by a red plus and minus sign, respectively. Abbreviations for parameters are explained in Table 1.

no straightforward linear or monotonic relationship. There also seems to be a trend for both seafloor roughness parameters, indicating that a rougher seafloor is associated with more tsunami events. This is confirmed by the significant ($p < 0.05$), relatively high ($\rho = 0.32$ for R_{sw} and $\rho = 0.30$ for R_{lw}) Spearman rank correlations for both R_{sw} and R_{lw}, although no significant, high correlations are found for the Pearson's coefficient. The two subduction zone segments with the highest normalised number of tsunami events N_t are Japan and South-Kuril. Because of their high N_t, they are often outliers.

There are no significant correlations between N_t and the distance between the volcanic arc and the trench $D_{\mathrm{arc-trench}}$ (which is a seismicity-independent proxy for the slab dip) or the upper plate strain UPS.

3 Multivariate statistical analysis: an in-depth look into relationships between tsunami events and subduction zone characteristics

3.1 Methods

The bivariate analysis presented in Section 2 suffers from the scarcity of the tsunami data. This is illustrated by the limited amount of significant correlation coefficients (i.e., $p < 0.05$) for both the Pearson's product-moment and the Spearman rank analyses. A multivariate approach, as described in this section, can help to further reveal the conditions promoting tsunamigenic earthquakes, despite the scarcity of the tsunami data.

Following *Sandri et al.* (2004) and *Brizzi et al.* (2018), we use the Fisher discriminant method (e.g., *Duda et al.*, 1973) to perform a pattern recognition analysis focused on discovering combinations of parameters that could promote the occurrence of earthquake-generated tsunami events (see *Van Zelst*, 2025, for the scripts used). We only consider the tectonic parameters of our SNITCH database to take advantage of all available tsunami data from 1962 – 2018 (*Global Historical Tsunami Database*, Retrieved: February 1, 2019). We exclude L^* from the tectonic parameters in our analysis, because this parameter solely depends on the choice of the subduction zone segments and does not represent a physical feature of the subduction system.

We first identify linear combinations that can divide the subduction zone segments in two classes based on N_t, with class 1 containing subduction zone segments with few earthquake-generated tsunami events (i.e., $N_t < 0.2$), and class 2 containing subduction zone segments with a large number of earthquake-generated tsunami events (i.e., $N_t \geq 0.2$). The threshold of 0.2 is chosen because it seems to naturally divide the data in the case of the bivariate analysis, as shown in the scatter plots of the age, sediment thickness, and type of margin in Figure 4. Using different thresholds ranging from 0–0.3 slightly changes the parameters that are most effective in dividing the two classes, but in general the combination of parameters is consistent.

The Fisher discriminant analysis typically consists of a learning phase, a voting phase, and control experiments (e.g., *Sandri et al.*, 2004, and references therein). However, following *Brizzi et al.* (2018), we confine our analysis to the learning phase due to the limited amount of data. During the learning phase, an input set of n parameters is used to identify all the possible linear combinations consisting of $k = 1, ..., n$ parameters. To distinguish the effect of multiple parameters that could be interdependent, we run 36 Fisher analyses to systematically test the effect of the parameters. The parameters A, $D_{\mathrm{arc-trench}}$, and UPS are independent parameters that are always included in the analysis. T_{sed} and $AvsE$ (i.e., the type of margin:

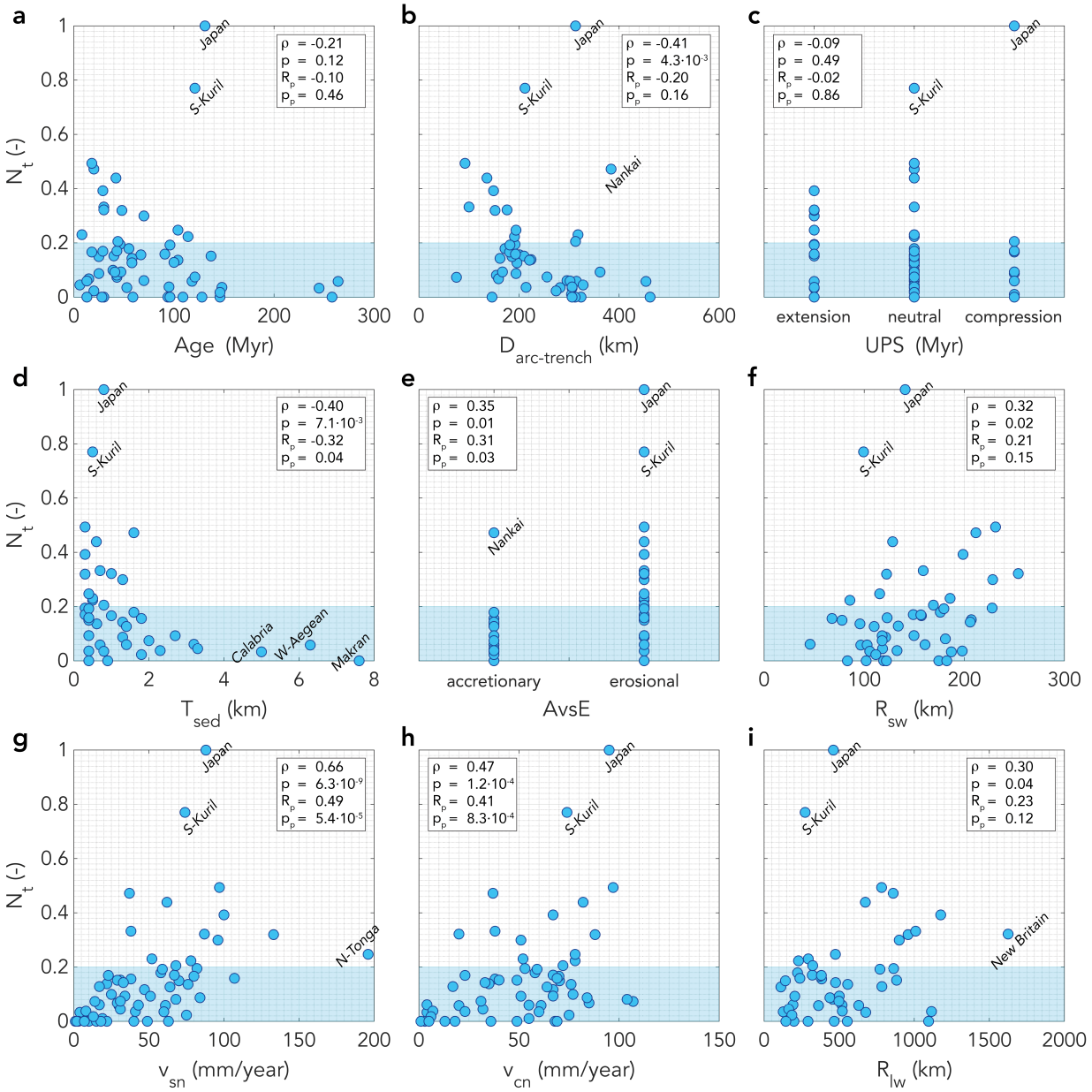

Figure 4 – Scatter plots showing the relation between the normalised number of earthquake-generated tsunami events per km trench N_t and (a) the age of the subducting plate A; (b) the distance between the volcanic arc and the trench $D_{\mathrm{arc-trench}}$; (c) the upper plate strain UPS; (d) the sediment thickness at the trench T_{sed}; (e) the type of margin $AvsE$; (f) the short wavelength (i.e., 12–20 km) roughness R_{sw}; (g) the trench-normal component of the subduction velocity v_{sn}; (h) the trench-normal component of the convergence velocity v_{cn}; and (i) the long wavelength (i.e., 80–100 km) roughness R_{lw}. Each dot represents one of the 62 subduction zone segments. Correlation coefficients and p-values are indicated for both the Spearman and Pearson methods. The names of the subduction zone segments are indicated for isolated points in the scatter plots. The threshold of 0.2 for the multivariate analysis is indicated by the blue rectangle. Abbreviations for parameters are explained in Table 1.

accretionary or erosional) are dependent on each other as larger sediment thickness is usually associated with accretionary margins, whereas small sediment thickness is typically associated with erosional margins. Therefore, we run three different test cases: one in which both parameters are included and two where each parameter is included separately. The same reasoning holds for the two measures of incoming plate roughness R_{sw} and R_{lw}. We adopt a similar reasoning for the velocities v_{sn}, v_{cn}, but we also include the option to exclude both velocities from the linear combination, because they could potentially relate to the limited time span of observations in addition to a physical mechanism. This then results in a total of $3 \cdot 3 \cdot 4 = 36$ different sets of input parameters for the Fisher analysis. For a given set of input parameters, there is one linear combination with a minimum number of parameters k_m that minimises the error: the optimal linear combination (Figure 5). For each analysis, we automatically detect this optimal linear combination when the error reduction by including more parameters into the analysis becomes less than 5% with respect to the initial error in the case of including only one parameter. Hence, we end up with an optimal linear combination for each of the 36 Fisher analyses. The coefficients in the linear combinations indicate the importance of a parameter in the combination.

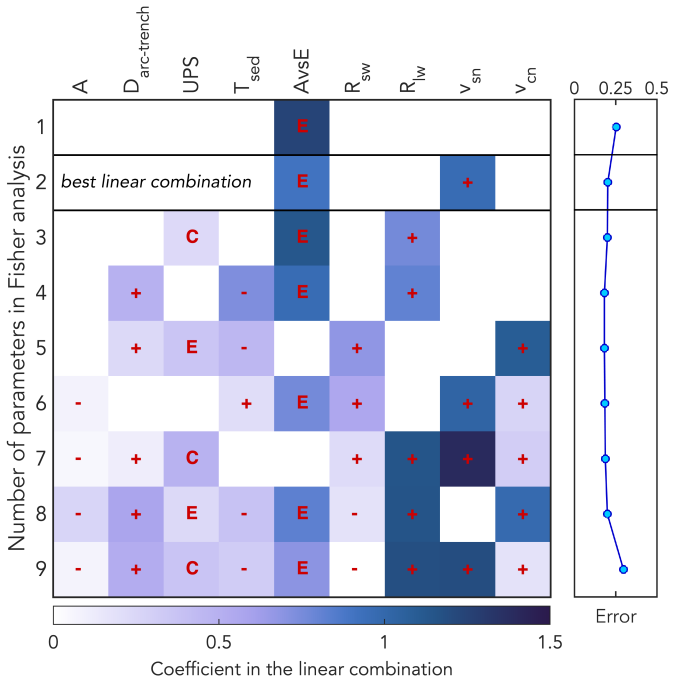

Figure 5 – Representative Fisher analysis for one set of input parameters (listed at the top). When a parameter is included in the linear combination, a red symbol indicates how it promotes class 2 ($N_t \geq 0.2$). Hence, a plus indicates that larger values of a parameter are associated with class 2. For discrete parameters, letters indicate the most favourable setting for class 2 (see Table 1). The right panel shows the error reduction when more parameters are included in the linear combination. The optimal linear combination for which the error is maximally reduced for the least amount of features included in the linear combination is indicated by black lines.

To systematically determine which parameters are the most important for generating tsunamigenic earthquakes, we look at three measures: (*i*) the fraction that a parameter is picked in the best linear combination for a Fisher analysis when it is part of the input; (*ii*) the normalised average coefficient of a parameter based on all Fisher analyses for which it is included in the best linear combination; (*iii*) the maximum fraction of a consistent sign (i.e., positive or negative) of the coefficient of a parameter to account for the robustness of the effect of the parameter in the linear combination. We define the measure of relative importance *RI* of a parameter as the multiplication of these three measures.

3.2 Results

3.2.1 An in-depth study of one representative Fisher analysis as an example

Figure 5 shows the results for one representative Fisher analysis. The input parameters used in the test are indicated at the top, and the resulting coefficients of the linear combinations for different numbers of parameters allowed in the linear combination (on the *y*-axis) is indicated by the colours in each row. Parameters are part of the linear combination when a red symbol is present in the relevant square.

If only one parameter is used to distinguish the two classes of few (class 1; $N_t < 0.2$) and many (class 2; $N_t \geq 0.2$) tsunamigenic earthquakes, the type of margin *AvsE* is the deciding factor. In this case, an erosional margin is more favourable to produce many tsunami events caused by earthquakes.

When a second parameter is allowed to enter the linear combination that divides the two classes, the trench-normal component of the subduction velocity is picked by the Fisher algorithm. The positive coefficient indicates that a large subduction velocity correlates to class 2, i.e., many earthquake-generated tsunami events. These two parameters, *AvsE* and v_{sn}, also exhibited high correlations in the bivariate analysis (Section 2.2). The combination of these two parameters is also the optimal linear combination as defined in Section 3.1. The error is namely reduced the most with respect to the least amount of features required to divide the two classes.

When a third parameter enters the linear combination, the upper plate strain *UPS* is picked by the Fisher analysis. An overriding plate that experiences compression is associated with many tsunami events. Simultaneously, the long wavelength roughness R_{lw} is picked instead of the subduction velocity, indicating that a rougher incoming plate is associated with the class of many tsunami events.

With four parameters, the upper plate strain is removed from the linear combination, and instead the sediment thickness T_{sed} and the distance between the volcanic arc and the trench $D_{\mathrm{arc-trench}}$ are picked. As $D_{\mathrm{arc-trench}}$ can be related to the dip of a slab, with large $D_{\mathrm{arc-trench}}$ being associated with a more shallowly dipping slab, a positive coefficient in the linear combination could hint at a relationship between shallowly dipping slabs and earthquake-generated tsunami events. The negative coefficient of the sediment thickness T_{sed} associated here with many tsunami events is in line with the erosional margin that is consistently present in almost all linear combinations.

When all 9 parameters are included in the linear combination, which is theoretically possible, the error is higher compared to the best linear combination. This indicates that including more parameters into the linear combination does not necessarily improve it.

Also note that the parameters chosen for the linear combinations can differ completely when a different number of parameters is allowed for the linear combination. The sign of the parameter can also change for different numbers of parameters. When the sign consistently remains the same over all linear combinations and Fisher analyses, we deem the effect of the parameter on dividing the two classes to be robust.

In summary, for the example Fisher analysis of Figure 5, the linear combination that best describes the difference between the two classes with these parameters as input consists of the type of margin and the subduction velocity.

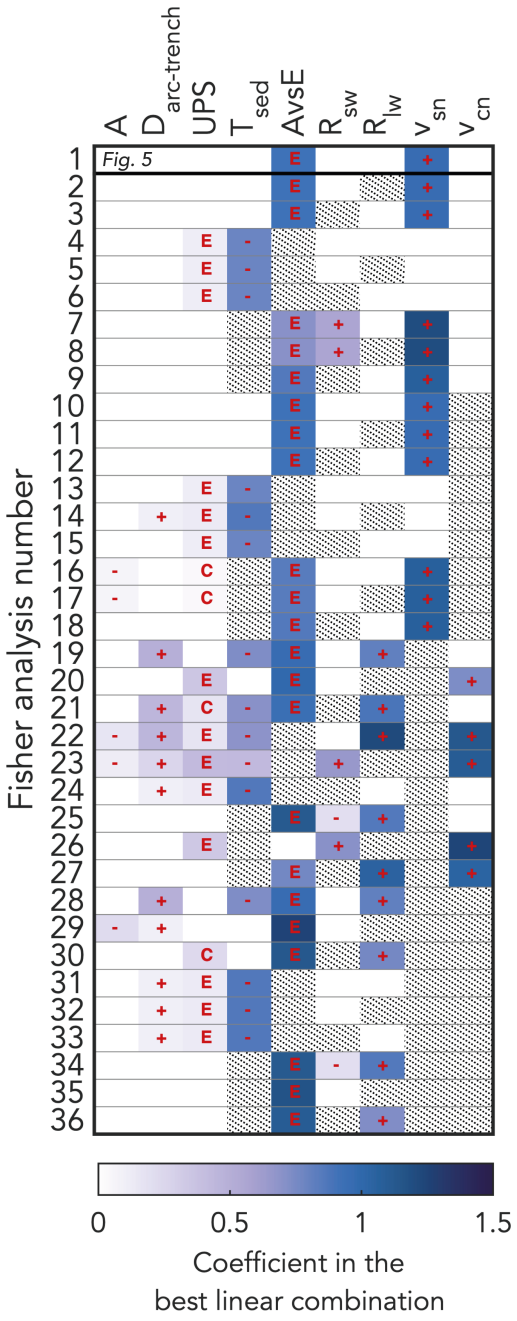

Figure 6 – The best linear combination for each Fisher analysis. When a parameter is included in the linear combination, a red symbol indicates how it promotes class 2 ($N_t \geq 0.2$). Hence, a plus indicates that larger values of a parameter are associated with class 2. For discrete parameters, letters indicate the most favourable setting for class 2 (see Table 1). If parameters are not included in the input for a test, the area is dotted. Note that the best linear combination of Figure 5 is included here as well and highlighted by horizontal black lines.

3.2.2 Combined results of all Fisher analyses

When we consider all 36 Fisher analyses, the amount of parameters included in the best linear combination is on average 2.9. The maximum amount of parameters included in the optimal linear combination is 6. The error associated with the best linear combination is on average 0.22. This corresponds to an average of 10.5 segments (25.6%) that are classified in the wrong class according to the optimal linear combination. The best linear combinations for each of the 36 Fisher analyses that were run for different combinations of input parameters are shown in Figure 6. Several variables appear to stand out, such as the type of margin (consistently erosional) and the subduction velocity (consistently positive). We summarise the main findings of these 36 analyses in Figure 7, by calculating the relative importance of each parameter as described in Section 3.1.

The most important parameter, with a relative importance of 0.86, is the type of margin, i.e., accretionary or erosional. When it is included in the input parameters of the Fisher analysis, it is picked 95.8% of the time in the best linear combination. After that, the second most important parameter is the trench-normal component of the subduction velocity with relative importance 0.66, which is picked 66.7% of the time. The third most important parameter is the sediment thickness with $RI = 0.46$, which is picked 50% of the time. The long wavelength roughness has a relative importance of 0.32 and the trench-normal component of the convergence velocity has $RI = 0.28$. The other parameters show low measures of relative importance with $RI < 0.1$. Hence, the Fisher analysis reveals the general pattern that from 1962 to 2018 earthquake-generated tsunami events occurred more frequently in subduction zones with an erosional margin with few sediments and a rough incoming seafloor in a

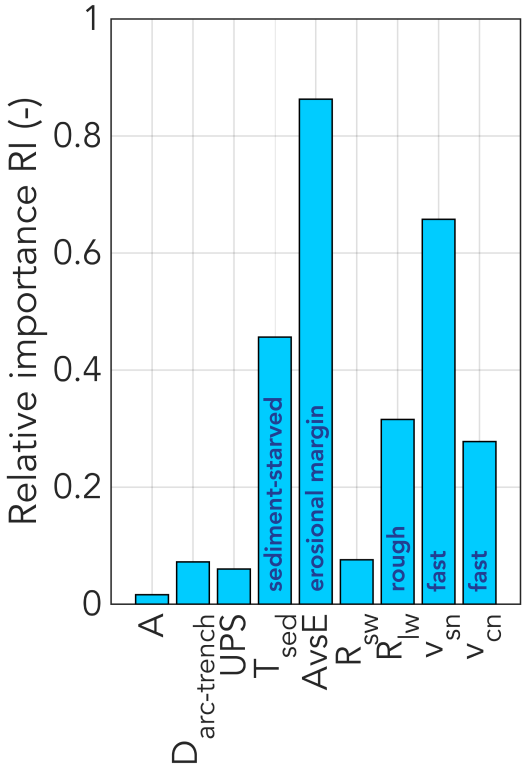

Figure 7 – The relative importance of parameters (Section 3.1) as calculated from the Fisher analyses presented in Figure 6. For parameters with a relative importance $RI > 0.2$, text in the bars indicates how the parameter promotes many earthquake-generated tsunami events (class 2).

rapidly converging system.

4 Discussion

We compiled the SNITCH database consisting of tsunami events and parameters on the megathrust seismicity, seismogenic zone geometry, and tectonic characteristics of subduction zones across the world.

We focus our study on the normalised number of tsunami events per km trench N_t, although the NOAA NGDC/WDS Global Historical Tsunami Database does contain other information on the extracted tsunami events caused by earthquakes. For instance, there is limited information on the maximum water height, tsunami magnitude and intensity, and focal depth of the earthquake that caused the tsunami. However, the data in the NOAA NGDC/WDS Global Historical Tsunami Database is scarce for each tsunami, meaning that no robust statistics can be built for these alternative parameters across subduction zones. Additionally, when values are present in the database for specific parameters, such as the maximum water height or tsunami intensity and magnitude, they have often been taken from different sources and are therefore not compatible with each other for the same tsunami. That is to say, the tsunami magnitude and intensity in the NOAA NGDC/WDS Global Historical Tsunami Database are not directly calculated from the maximum water height that is also scarcely reported in the database. In addition, it is important to take into account that these variables are not necessarily comparable to each other across multiple events and regions, since they might use different definitions of the maximum water height and are highly dependent on local bathymetry. Hence by focusing our analysis on the normalised number of tsunami events per km trench N_t we ensure that the results we present and the analyses that we do are statistically significant.

Generally the amount of tsunami events depends on the amount of large earthquakes that has occurred in a subduction zone. This is captured in our analysis, as we find significant correlations in the bivariate analysis (Section 2) between N_t and various measures of the maximum earthquake magnitude a subduction zone segment has experienced. This indicates the robustness of N_t as a useful measure for tsunamigenic potential in subduction zones.

The bivariate analysis further shows that the normalised number of tsunami events per km trench N_t correlates with some of the interplate seismicity and tectonic parameters in our SNITCH database. Specifically, meaningful correlations are found with the type of margin (i.e., accretionary or erosional), the trench-normal components of the subduction and convergence velocity of the subduction zone, the sediment thickness, seismicity rate, and measures of maximum earthquake magnitude in a subduction zone segment. However, N_t shows no correlation with the geometric parameters describing the seismogenic zone.

The multivariate analysis of the tectonic parameters points towards the same parameters identified in the bivariate analysis and to the incoming plate roughness, to distinguish subduction zones with a lower ($N_t < 0.2$) and higher number of earthquake-generated tsunami events ($N_t \geq 0.2$). Specifically, we find that rough incoming plates at erosional margins, in rapidly converging systems have produced more earthquake-generated tsunami events during the analysed time span.

In the following, we put our results in the context of the limitations of and assumptions in our approach and compare with existing literature. As such, we discuss which — if any — tectonic setting is more favourable for tsunamigenic earthquakes and how this could affect tsunamigenesis according to our analysis. We also speculate which kind of fault is likely to be the most important in producing tsunamigenic earthquakes, as we did not find a correlation with the seismogenic zone geometry parameters.

4.1 Are there any specific tectonic settings where more earthquake-generated tsunami events have been observed?

We find multiple significant correlations and patterns in both the bivariate and multivariate analyses, indicating that certain parameters are indeed correlated with an increased amount of observed tsunami events. So, we show that there are indeed specific tectonic settings where more earthquake-generated tsunami events have been observed from 1962 to 2018. Therefore, we speculate that there are specific tectonic settings that could be more prone to host tsunamigenic earthquakes (Section 4.2). However, it is important to note that most scatter plots still contain outliers (Figure 4) and there are always at least 8 segments (12.9%) incorrectly classified in the multivariate analysis (Section 3.2). Besides that, for some parameters no clear correlation can be discerned at all. This is partly due to the limited amount of data for the 62 subduction zone segments. Most parameters in the SNITCH database do not have values for each subduction zone segment due to a lack of observations.

In addition, we only consider a limited observational time span for the data in this study, with the tsunami data limited to 1962–2018. This time span is constrained by the availability of as-complete-as-possible global coverage of tsunami observations, as recommended by the *Global Historical Tsunami Database* (Retrieved: February 1, 2019). Incorporating data from outside this observational time window would skew the results of our statistical analysis by adding a bias towards tsunami events caused by large magnitude earthquakes that are more easily observable. However, as a downside, this means that the tsunamigenic potential of regions that have experienced large earthquake-generated tsunamis outside of the time frame of our database might be underestimated in our analysis (also see Section 1.2).

Interestingly, the seismogenic zone geometry parameters (Section 2.2) do not correlate with N_t in our bivariate analysis, which can have different explanations. First, it might be that the amount of

data present in our tsunami databases is too scarce to result in any significant correlation (Figure 3). However, other parameters do show significant correlations, so this option is not necessarily true. An alternative explanation might be that the megathrust is not the only important fault in tsunamigenesis. Because of that, the seismogenic zone parameters that define the potential slip area on the megathrust do not correlate with N_t. We explore this option in more detail in Section 4.3.

Our bivariate study shows a relationship between the number of tsunami events and the maximum earthquake magnitude. Through the Gutenberg-Richter statistics of earthquakes (*Gutenberg and Richter*, 1956), this is straightforwardly explained through the fact that a larger earthquake magnitude implies more (potentially tsunamigenic) aftershocks. In addition, larger earthquakes have a higher tsunamigenic potential through their potential for larger surface displacement. We must therefore presume that there is an established relationship between the recurrence interval of large earthquakes in a region and large tsunami events. We attempt to eliminate this effect of the recurrence interval of regions on tsunamigenic behaviour by looking at the normalised number of tsunami events per km trench N_t for the time frame from 1962 – 2018, for which globally reliable tsunami observations are available. However, this time frame is less than the recurrence intervals of large earthquakes, which can be up to a few hundred years (*Goldfinger et al.*, 2003; *Cisternas et al.*, 2005; *Sieh et al.*, 2008; *Goldfinger et al.*, 2013; *Brizzi et al.*, 2020). Hence, despite using the most comprehensive and homogenised dataset available, our approach might not fully capture correlations between tectonic parameters and tsunamigenesis due to the limited tsunami record.

Concerning the parameter N_t on which we base our main analysis, we believe it provides a scale-free measure to quantify the tsunamigenic activity of a region. This allows us to perform our statistical analysis to see if there are any correlations between tectonic and tsunami parameters. However, as mentioned before, N_t is not a perfect measure of tsunamigenic activity and indeed misses a lot of the physics that we know governs tsunamigenesis to an extent. Therefore, while our findings highlight the existence of trends, it is possible that correlations and inferred relationships could evolve in the future as more comprehensive tsunami datasets or alternative, more 'physically driven' tsunami parameters become available at the global scale (also see Section 1.2).

4.2 Which tectonic parameters are correlated to an increased number of earthquake-generated tsunami events in subduction zones?

Our analysis shows that subduction zones where a rough incoming plate subducts rapidly at an erosional margin are generally more likely to have hosted many earthquake-generated tsunami events from 1962 – 2018 than their slowly subducting, smooth, accretionary counterparts (Figure 8).

Indeed, the Japan subduction zone segment, which has the highest normalised number of tsunami events per km trench from 1962 to 2018, is an erosional margin with low sediment cover (0.8 km sediment thickness at the trench) and a moderate long-wavelength roughness of 461.24 km (Figure 4). The Southern Kuril subduction segment, which also has a high N_t of 0.77, shares those characteristics with the Japan subduction segment, with a trench sediment thickness of 0.5 km and a slightly lower long-wavelength roughness of 273.31 km. In contrast, subduction segments with a notably high sediment thickness, such as the Calabria (5.0 km), West Aegean (6.3 km), and Makran (7.6 km) subduction zones, show very low values of N_t (Figure 4), although it is important to note that significant earthquake-generated tsunami events have occurred in some of these settings in the past, outside the time window of our database. Apart from a low sediment thickness, the Calabria subduction segment is also an accretionary setting and has low convergence velocities with $v_{cn} = 4$ mm year^{-1} and $v_{sn} = 4$ mm year^{-1}. The West Aegean and Makran subduction segments are also accretionary margins, but sport slightly higher convergence velocities up to a few cm per year. The subduction zone with the highest long-wavelength roughness, New Britain, has a moderate value of N_t of 0.32 and — in line with our general results — is an erosional margin with low sediment cover at the trench (1.0 km) and a high subduction velocity of $v_{sn} = 87$ mm year^{-1}.

Our findings are also in line with other studies, which show that tsunami earthquakes are typically associated with erosional margins (*Polet and Kanamori*, 2000; *Bilek*, 2010; *Geersen*, 2019; *Meng and Duan*, 2023) and a rough incoming plate (*Bell et al.*, 2014; *Geersen*, 2019). Our analysis also highlights the importance of having a thin sediment layer in the subduction segment in order to be associated with more tsunamigenic earthquakes. The effect of a thin sediment layer on tsunamigenic earthquake occurrence in subduction zones fits well with the importance of erosional margins, because sediment-starved trenches are often associated with erosional margins. However, this does not mean that erosional margins are completely devoid of sediment cover (*Clift and Vannucchi*, 2004). It has been suggested that the presence of sediments could enhance tsunamigenesis, by promoting larger uplift (*Ma and Nie*, 2019). This could explain the large range of N_t for subduction zone segments with moderate sediment cover (i.e., $T_{\text{sed}} \leq 2$ km; Figure 4d). Therefore, erosional margins with a small sedimentary wedge may be more prone to host tsunamigenic earthquakes. The negative correlation between sediment thickness and the amount of normalised tsunami events in a subduction zone segment could also be related to the effect of sediment thickness on the recurrence time of earthquakes. For example, the modelling study of *Brizzi et al.* (2020) shows that less sediment cover results in a smaller seismogenic zone with a shorter recurrence interval. Here, we find that subduction zone segments with a thick sedimentary layer — and, presumably, a larger recurrence interval — have generally produced

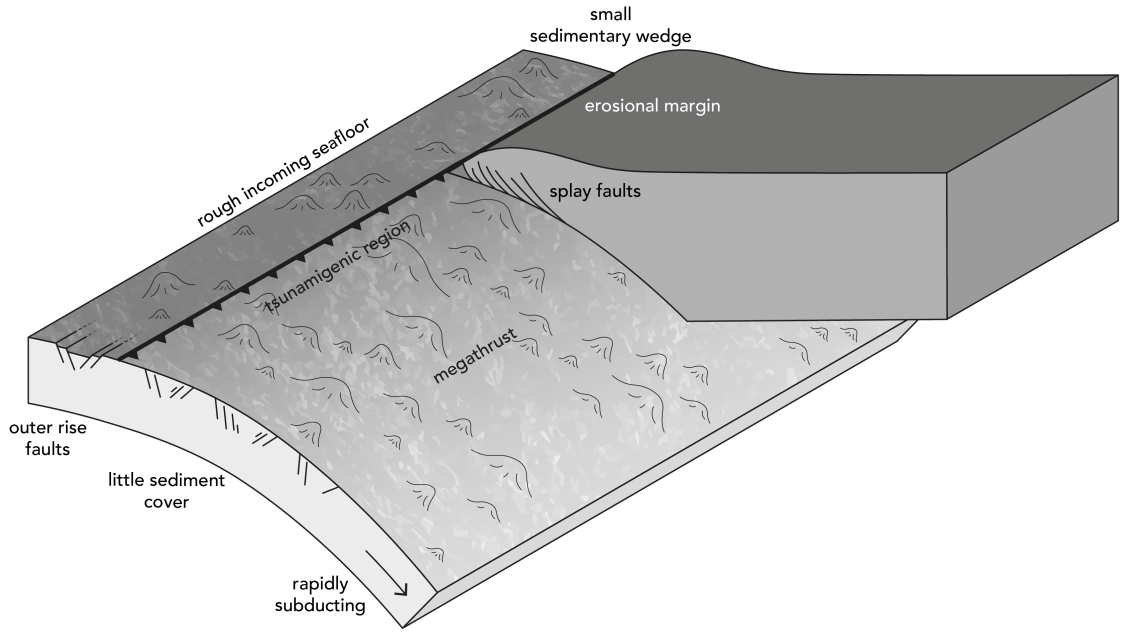

Figure 8 – Illustration of a tectonic setting that is potentially more prone to host tsunamigenic earthquakes according to our analysis: a subducting plate with little sediments and a rough incoming seafloor subducts relatively rapidly beneath a continental plate at an erosional margin.

less tsunamis, which could be a result of the limited observational time span of the SNITCH database (Section 4.1). One outlier that is apparent in Figure 4e is the Nankai subduction segment, which has produced relatively many tsunami events even though it is an accretionary margin rather than erosional. However, the Nankai segment has experienced periods of erosion (*Clift and Vannucchi*, 2004), which might explain why it has experienced more tsunami events than the other accretionary margins. The Nankai subduction segment is also characterised by a rough subducting plate with many topographical features such as seamounts (*Yokota et al.*, 2016). Since we find that rough subducting plates are associated with more tsunamigenic earthquakes, this could also contribute towards the reason as to why Nankai is an outlier.

The importance of the trench-normal components of the subduction and convergence velocity can be explained through the general relationship between earthquakes and tsunamis also found in the bivariate analysis (Section 2.2; Figure 3). In a subduction zone with a high subduction or convergence velocity, the stresses are built up faster and hence released more often in earthquakes, resulting in a shorter recurrence interval. More earthquakes generally means a larger likelihood of those earthquakes producing tsunamis. Since our study is restricted to a specific time interval for tsunamigenic earthquake observations, it is indeed likely that the subduction zones with a higher convergence velocity have produced more tsunamigenic earthquakes in this time period (*McCaffrey*, 2008; *Corbi et al.*, 2017). An alternative explanation for the importance of the velocities could be that large convergence velocities are typically associated with erosional margins (*Clift and Vannucchi*, 2004). Since we find that erosional margins are the most important factor for increased tsunamigenesis, it follows that the two aspects associated most with erosional margins, i.e., fast convergence and a thin sediment cover, are also highlighted in our analysis as important factors for tsunamigenesis.

As mentioned before, other studies have already linked sediment thickness at the trench and seafloor roughness to tsunami earthquakes (e.g., *Tanioka et al.*, 1997; *Polet and Kanamori*, 2000; *Bilek*, 2010; *Bell et al.*, 2014; *Geersen*, 2019; *Wang and Lin*, 2022; *Meng and Duan*, 2023). The combination of a thin sediment layer at the trench and a rough seafloor in particular has already been pointed out for 13 tsunami earthquake regions at 7 different subduction zones (i.e., Sumatra, Java, Hokkaido and the Kurils, Aleutians, Nicaragua, Peru, and New Zealand) by *Geersen* (2019). They looked at structural similarities between marine acoustic data. Our study strengthens this view by providing the first global, statistical analysis of the effect of these parameters on tsunamigenic earthquakes, which include both tsunami earthquakes and large megathrust earthquakes that caused tsunamis. The amount of trench sediments and the roughness of the seafloor are often considered as related, because thick piles of sediment entering the trench could potentially smooth out the topography on the incoming plate (*Ruff*, 1989; *Van Rijsingen et al.*, 2018). It is generally thought that a rough incoming seafloor and lack of sediments leads to a complex, heavily fractured shallow subduction interface (*Dominguez et al.*, 1998; *Wang and Bilek*, 2011, 2014; *Ruh et al.*, 2016). Such a heavily fractured environment could promote tsunami(genic) earthquakes, because of the increased presence of outer rise and splay faults that

can already accommodate large vertical displacements for smaller earthquake magnitudes.

4.3 Which type of fault produces tsunamigenic earthquakes?

It has long been known that the megathrust plays a crucial role in tsunamigenesis. As the largest potential rupture plane in a subduction zone, the megathrust can host large earthquakes under the right conditions (e.g., a flat and smooth megathrust has been shown to be more prone to hosting large earthquakes; *Heuret et al.*, 2011; *Wang and Bilek*, 2014; *Bletery et al.*, 2016). These large events often cause sufficient seafloor uplift to generate a corresponding tsunami.

However, earthquake size is not the only factor influencing tsunamigenesis (*Satake and Tanioka*, 1999). Indeed, tsunami events are not necessarily solely associated with the megathrust. Tsunami events are also often associated with earthquakes that potentially ruptured outer rise or splay faults, such as the 1933 M_w 8.4 Sanriku (*Kanamori*, 1971), 1946 Unimak Alaska (*von Huene et al.*, 2016), and 2006 Java (*Fan et al.*, 2017) tsunami earthquakes. Simultaneously, splay faults could also play a role during large megathrust earthquakes, as suggested for the 2004 M_w 9.1–9.3 Sumatra-Andaman (*DeDontney and Rice*, 2012; *Waldhauser et al.*, 2012) and the 2010 M_w 8.8 Maule (*Melnick et al.*, 2012) earthquakes.

Our study shows a lack of correlations between N_t and the seismogenic zone geometry parameters in our bivariate analysis, as discussed in Section 4.1. This could potentially indicate that the megathrust is not the only important fault when it comes to producing tsunamigenic earthquakes. Indeed, many studies have proposed that outer rise or splay faults play an important role for tsunamigenesis (e.g., *Fukao*, 1979; *Wendt et al.*, 2009; *Hubbard et al.*, 2015; *Sladen and Trevisan*, 2018; *Hananto et al.*, 2020; *Qiu and Barbot*, 2022; *Van Zelst et al.*, 2022). Slip on these types of faults, which are typically steeper than the megathrust, could result in larger vertical displacement compared to megathrust events. This could explain the discrepancy between earthquake moment magnitude and tsunami magnitude observed during tsunami earthquakes (*Kanamori*, 1972a). We speculate that faults other than the megathrust might play an equally, or more, important role in tsunamigenesis.

To fully tease out if there are any correlations between the presence of steeper outer rise or splay faults and increased tsunamigenic potential, future studies could focus on in-depth, regional assessments of faulting structures in the incoming and overriding plates and use finite fault inversions and focal mechanisms of tsunamigenic earthquakes to distinguish between the type of fault on which they occurred.

5 Conclusions

We compiled the SNITCH database, which contains global data on earthquake and tectonic subduction zone features, and earthquake-generated tsunami events for 62 subduction segments. In the performed bivariate analysis, we find correlations between the normalised number of earthquake-generated tsunami events per km trench N_t and some of the tectonic parameters, namely, the type of margin: accretionary or erosional, the trench-normal components of the subduction and convergence velocity, and the sediment thickness at the trench.

The multivariate analysis explores the relationships between the tectonic parameters and the tsunamigenic potential of a subduction zone further. The type of margin (i.e., erosional or accretionary) and the subduction and convergence velocity normal to the trench are the most crucial parameters to sort the subduction zones between a class with few tsunami events ($N_t < 0.2$) and a class with many tsunami events ($N_t \geq 0.2$). Parameters of secondary importance for this division are the long wavelength roughness and the sediment thickness at the trench. Tsunamigenic earthquakes therefore appear to be more common in rapidly converging, erosional subduction settings, with a rough incoming plate and low amounts of sediments at the trench. These settings are characterised by heavily fractured and complex, heterogeneous shallow subduction interfaces arising from the rough seafloor and the lack of sediments smoothing the interface. Tsunamigenic earthquakes may be more common in such settings, because of the presence of more splay faults, which could accommodate larger vertical displacements. However, we caution that our multivariate analysis only considers the normalised number of earthquake-generated tsunami events per km trench N_t as a measure of tsunamigenesis, because it is the only reliable globally available metric. This ignores the size of the tsunami and the correlation between tsunami excitation and earthquake recurrence. In the future, more quantitative tsunami measures of the tsunami energy per fault length would be ideal to characterise the relationship between the tectonics of a region and its tsunamigenic potential.

Acknowledgements

We would like to thank editor Craig Magee, associate editor Jack Williams, and reviewers Jonathan Griffin and Qiang Qiu for constructive feedback that improved the manuscript. We would like to thank Andreas Fichtner for fruitful discussions and support that greatly improved this work. We are also grateful to Arnauld Heuret, Claudia Piromallo, and Serge Lallemand, for providing and helping with the subduction zone parameters of the SNITCH database. We thank Laura Sandri for helping to set up the Fisher analysis.This work is part of the ASCETE project funded by the Volkswagen Foundation (Advanced Simulation of Coupled Earthquake-Tsunami Events, grant no 88479). FF, SB, and EvR were supported by the FIS project SCALEMOD, EPOS ITALIA, PNRR-MEET, and the grant to the Department of Science at Roma Tre University (MUR-Italy Dipartimenti di Eccellenza).

EvR also received funding from the European Union's Horizon 2020 research and innovation programme under the Marie Sklodowska-Curie grant agreement No 101032311 - SEGMENT. IvZ acknowledges the financial support and endorsement from the DLR Management Board Young Research Group Leader Program and the Executive Board Member for Space Research and Technology. Throughout this work, we use scientific colour maps by *Crameri* (2018) to prevent visual distortion of the data and exclusion of readers with colour-vision deficiencies (*Crameri et al.*, 2020).

Author contributions

Conceptualization - I. van Zelst
Methodology - I. van Zelst, S. Brizzi
Data Curation - I. van Zelst, S. Brizzi, E. van Rijsingen
Formal Analysis - I. van Zelst
Writing - Original draft - I. van Zelst
Writing - Review & Editing - I. van Zelst, S. Brizzi, E. van Rijsingen, F. Funiciello, Y. van Dinther
Visualization - I. van Zelst
Supervision - F. Funiciello, Y. van Dinther
Funding Acquisition - F. Funiciello, Y. van Dinther

Data availability

The SNITCH database, coordinates of the subduction zone segments, and MATLAB scripts to reproduce this study can be found in *Van Zelst* (2025).

Competing interests

The authors declare no competing interests.

Peer review

This publication was peer-reviewed by Jonathan Griffin and Qiang Qiu. The full peer-review report can be found here: Review Report.

Copyright notice

References

Bell, R., C. Holden, W. Power, X. Wang, and G. Downes (2014), Hikurangi margin tsunami earthquake generated by slow seismic rupture over a subducted seamount, *Earth and Planetary Science Letters*, *397*, 1 – 9, doi: 10.1016/j.epsl.2014.04.005.

Bilek, S. L. (2010), The role of subduction erosion on seismicity, *Geology*, *38*(5), 479–480, doi: 10.1130/focus052010.1.

Bletery, Q., A. M. Thomas, A. W. Rempel, L. Karlstrom, A. Sladen, and L. De Barros (2016), Mega-earthquakes rupture flat megathrusts, *Science*, *354*(6315), 1027–1031, doi: 10.1126/science.aag0482.

Brizzi, S., L. Sandri, F. Funiciello, F. Corbi, C. Piromallo, and A. Heuret (2018), Multivariate statistical analysis to investigate the subduction zone parameters favoring the occurrence of giant megathrust earthquakes, *Tectonophysics*, *728*, 92–103, doi: 10.1016/j.tecto.2018.01.027.

Brizzi, S., I. Van Zelst, F. Funiciello, F. Corbi, and Y. van Dinther (2020), How sediment thickness influences subduction dynamics and seismicity, *Journal of Geophysical Research: Solid Earth*, *125*(8), e2019JB018,964, doi: 10.1029/2019JB018964.

Carvajal, M., T. Sun, K. Wang, H. Luo, and Y. Zhu (2022), Evaluating the Tsunamigenic Potential of Buried Versus Trench-Breaching Megathrust Slip, *Journal of Geophysical Research: Solid Earth*, *127*(8), e2021JB023,722, doi: 10.1029/2021JB023722.

Cisternas, M., B. F. Atwater, F. Torrejón, Y. Sawai, G. Machuca, M. Lagos, A. Eipert, C. Youlton, I. Salgado, T. Kamataki, et al. (2005), Predecessors of the giant 1960 Chile earthquake, *Nature*, *437*(7057), 404, doi: 10.1038/nature03943.

Clift, P., and P. Vannucchi (2004), Controls on tectonic accretion versus erosion in subduction zones: Implications for the origin and recycling of the continental crust, *Reviews of Geophysics*, *42*(2), doi: 10.1029/2003RG000127.

Corbi, F., F. Funiciello, S. Brizzi, S. Lallemand, and M. Rosenau (2017), Control of asperities size and spacing on seismic behavior of subduction megathrusts, *Geophysical Research Letters*, *44*, doi: 10.1002/2017GL074182.

Crameri, F. (2018), Scientific colour-maps, doi: 10.5281/zenodo.1243862.

Crameri, F., G. E. Shephard, and P. J. Heron (2020), The misuse of colour in science communication, *Nature communications*, *11*(1), 1–10, doi: 10.1038/s41467-020-19160-7.

DeDontney, N., and J. R. Rice (2012), Tsunami wave analysis and possibility of splay fault rupture during the 2004 Indian Ocean earthquake, *Pure and applied geophysics*, *169*(10), 1707–1735, doi: 10.1007/s00024-011-0438-4.

Delouis, B., J.-M. Nocquet, and M. Vallée (2010), Slip distribution of the February 27, 2010 M_w = 8.8 Maule Earthquake, central Chile, from static and high-rate GPS, InSAR, and broadband teleseismic data: slip disturbance Maule earthquake, *Geophysical research letters*, *37*(17), doi: 10.1029/2010gl043899.

DeMets, C., R. G. Gordon, D. Argus, and S. Stein (1990), Current plate motions, *Geophysical journal international*, *101*(2), 425–478, doi: 10.1111/j.1365-246X.1990.tb06579.x.

Dominguez, S., S. Lallemand, J. Malavieille, and R. von Huene (1998), Upper plate deformation associated with seamount subduction, *Tectonophysics*, *293*(3-4), 207–224, doi: 10.1016/S0040-1951(98)00086-9.

Duda, R. O., P. E. Hart, and D. G. Stork (1973), *Pattern classification and scene analysis*, vol. 3, Wiley New York.

Fan, W., D. Bassett, J. Jiang, P. M. Shearer, and C. Ji (2017), Rupture evolution of the 2006 Java tsunami earthquake and the possible role of splay faults, *Tectonophysics*, *721*,

143–150, doi: 10.1016/j.tecto.2017.10.003.

Fujii, Y., K. Satake, S. Sakai, M. Shinohara, and T. Kanazawa (2011), Tsunami source of the 2011 off the Pacific coast of Tohoku Earthquake, *Earth, planets and space*, *63*(7), 55, doi: 10.5047/eps.2011.06.010.

Fukao, Y. (1979), Tsunami earthquakes and subduction processes near deep-sea trenches, *Journal of Geophysical Research: Solid Earth*, *84*(B5), 2303–2314, doi: 10.1029/JB084iB05p02303.

Gahalaut, V., C. Subrahmanyam, B. Kundu, J. Catherine, and A. Ambikapathy (2010), Slow rupture in Andaman during 2004 Sumatra–Andaman earthquake: a probable consequence of subduction of 90E ridge, *Geophysical Journal International*, *180*(3), 1181–1186, doi: 10.1111/j.1365-246X.2009.04449.x.

Geersen, J. (2019), Sediment-starved trenches and rough subducting plates are conducive to tsunami earthquakes, *Tectonophysics*, *762*, 28–44, doi: 10.1016/j.tecto.2019.04.024.

Global Historical Tsunami Database (Retrieved: February 1, 2019), National Geophysical Data Center / World Data Service (NGDC/WDS), https://doi.org/10.7289/V5PN93H7.

Goldfinger, C., C. H. Nelson, J. E. Johnson, and S. S. Party (2003), Holocene earthquake records from the Cascadia subduction zone and northern San Andreas fault based on precise dating of offshore turbidites, *Annual Review of Earth and Planetary Sciences*, *31*(1), 555–577, doi: 10.1146/annurev.earth.31.100901.141246.

Goldfinger, C., Y. Ikeda, R. S. Yeats, and J. Ren (2013), Superquakes and supercycles, *Seismological Research Letters*, *84*(1), 24–32, doi: 10.1785/0220110135.

Gusiakov, V. K., P. K. Dunbar, and N. Arcos (2019), Twenty-five years (1992–2016) of global tsunamis: Statistical and analytical overview, *Pure and Applied Geophysics*, pp. 1–13, doi: 10.1007/s00024-019-02113-7.

Gutenberg, B., and C. F. Richter (1956), Magnitude and energy of earthquakes, *Annals of Geophysics*, *9*(1), 1–15, doi: 10.4401/ag-5590.

Hananto, N., F. Leclerc, L. Li, M. Etchebes, H. Carton, P. Tapponnier, Y. Qin, P. Avianto, S. Singh, and S. Wei (2020), Tsunami earthquakes: Vertical pop-up expulsion at the forefront of subduction megathrust, *Earth and Planetary Science Letters*, *538*, 116,197, doi: 10.1016/j.epsl.2020.116197.

Hayes, G. P. (2017), The finite, kinematic rupture properties of great-sized earthquakes since 1990, *Earth and Planetary Science Letters*, *468*, 94–100, doi: 10.1016/j.epsl.2017.04.003.

Hayes, G. P., D. J. Wald, and R. L. Johnson (2012), Slab1.0: A three-dimensional model of global subduction zone geometries, *Journal of Geophysical Research: Solid Earth*, *117*(B1), doi: 10.1029/2011JB008524.

Heidarzadeh, M., and K. Satake (2015), New insights into the source of the Makran tsunami of 27 November 1945 from tsunami waveforms and coastal deformation data, *Pure and Applied Geophysics*, *172*, 621–640, doi: 10.1007/s00024-014-0948-y.

Heuret, A., S. Lallemand, F. Funiciello, C. Piromallo, and C. Faccenna (2011), Physical characteristics of subduction interface type seismogenic zones revisited, *Geochemistry, Geophysics, Geosystems*, *12*(1), doi: 10.1029/2010GC003230.

Heuret, A., C. Conrad, F. Funiciello, S. Lallemand, and L. Sandri (2012), Relation between subduction megathrust earthquakes, trench sediment thickness and upper plate strain, *Geophysical Research Letters*, *39*(5), doi: 10.1029/2011GL050712.

Hubbard, J., S. Barbot, E. M. Hill, and P. Tapponnier (2015), Coseismic slip on shallow décollement megathrusts: Implications for seismic and tsunami hazard, *Earth-Science Reviews*, *141*, 45–55, doi: 10.1016/j.earscirev.2014.11.003.

Jiang, Y., P. J. González, and R. Bürgmann (2022), Subduction earthquakes controlled by incoming plate geometry: The 2020 M> 7.5 Shumagin, Alaska, earthquake doublet, *Earth and Planetary Science Letters*, *584*, 117,447, doi: 10.1016/j.epsl.2022.117447.

Kanamori, H. (1971), Seismological evidence for a lithospheric normal faulting – The Sanriku earthquake of 1933, *Physics of the Earth and Planetary Interiors*, *4*(4), 289–300, doi: 10.1016/0031-9201(71)90013-6.

Kanamori, H. (1972a), Mechanism of tsunami earthquakes, *Physics of the earth and planetary interiors*, *6*(5), 346–359, doi: 10.1016/0031-9201(72)90058-1.

Kanamori, H. (1972b), Tectonic implications of the 1944 Tonankai and the 1946 Nankaido earthquakes, *Physics of the Earth and Planetary Interiors*, *5*, 129–139, doi: 10.1016/0031-9201(72)90082-9.

Kanamori, H., and J. J. Cipar (1974), Focal process of the great Chilean earthquake May 22, 1960, *Physics of the Earth and Planetary Interiors*, *9*(2), 128–136, doi: 10.1016/0031-9201(74)90029-6.

Lallemand, S., M. Peyret, E. Van Rijsingen, D. Arcay, and A. Heuret (2018), Roughness characteristics of oceanic seafloor prior to subduction in relation to the seismogenic potential of subduction zones, *Geochemistry, Geophysics, Geosystems*, *19*(7), 2121–2146, doi: 10.1029/2018GC007434.

Lay, T., H. Kanamori, C. J. Ammon, M. Nettles, S. N. Ward, R. C. Aster, S. L. Beck, S. L. Bilek, M. R. Brudzinski, R. Butler, et al. (2005), The great Sumatra-Andaman earthquake of 26 December 2004, *Science*, *308*(5725), 1127–1133, doi: 10.1126/science.1112250.

López, A. M., and E. A. Okal (2006), A seismological reassessment of the source of the 1946 Aleutian 'tsunami' earthquake, *Geophysical Journal International*, *165*(3), 835–849, doi: 10.1111/j.1365-246X.2006.02899.x.

Ma, S., and S. Nie (2019), Dynamic wedge failure and along-arc variations of tsunamigenesis in the Japan Trench margin, *Geophysical Research Letters*, doi: 10.1029/2019GL083148.

McCaffrey, R. (2008), Global frequency of magnitude 9 earthquakes, *Geology*, *36*(3), 263–266, doi: 10.1130/G24402A.1.

Melnick, D., M. Moreno, M. Motagh, M. Cisternas, and R. L. Wesson (2012), Splay fault slip during the M_w 8.8 2010 Maule Chile earthquake, *Geology*, *40*(3), 251–254, doi: 10.1130/G32712.1.

Meng, Q., and B. Duan (2023), Do upper-plate material properties or fault frictional properties play more important roles in tsunami earthquake characteristics?, *Tectonophysics*, *850*, 229,765, doi: 10.1016/j.tecto.2023.229765.

Oryan, B., and W. R. Buck (2020), Larger tsunamis from megathrust earthquakes where slab dip is reduced, *Nature Geoscience*, *13*(4), 319–324, doi: 10.1038/s41561-020-0553-x.

Ozawa, S., T. Nishimura, H. Suito, T. Kobayashi, M. Tobita, and T. Imakiire (2011), Coseismic and postseismic slip of the 2011 magnitude-9 Tohoku-Oki earthquake, *Nature*, *475*(7356), 373, doi: 10.1038/nature10227.

Polet, J., and H. Kanamori (2000), Shallow subduction zone earthquakes and their tsunamigenic potential, *Geophysical Journal International*, *142*(3), 684–702, doi: 10.1046/j.1365-246x.2000.00205.x.

Qiu, Q., and S. Barbot (2022), Tsunami excitation in the outer wedge of global subduction zones, *Earth-science reviews*, *230*, 104,054, doi: 10.1016/j.earscirev.2022.104054.

Robinson, D., S. Das, and A. Watts (2006), Earthquake rupture stalled by a subducting fracture zone, *Science*, *312*(5777), 1203–1205, doi: 10.1126/science.1125771.

Ruff, L., and H. Kanamori (1980), Seismicity and the subduction process, *Physics of the Earth and Planetary Interiors*, *23*(3), 240–252, doi: 10.1016/0031-9201(80)90117-X.

Ruff, L. J. (1989), Do trench sediments affect great earthquake occurrence in subduction zones?, in *Subduction Zones Part II*, pp. 263–282, Springer, doi: 10.1007/BF00874629.

Ruh, J. B., V. Sallarès, C. R. Ranero, and T. Gerya (2016), Crustal deformation dynamics and stress evolution during seamount subduction: High-resolution 3-D numerical modeling, *Journal of Geophysical Research: Solid Earth*, *121*(9), 6880–6902, doi: 10.1002/2016JB013250.

Sandri, L., W. Marzocchi, and L. Zaccarelli (2004), A new perspective in identifying the precursory patterns of eruptions, *Bulletin of volcanology*, *66*(3), 263–275, doi: 10.1007/s00445-003-0309-7.

Satake, K. (2015), 4.19 - Tsunamis, in *Treatise on Geophysics*, edited by G. Schubert, second ed., pp. 477 – 504, Elsevier, Oxford, doi: 10.1016/B978-0-444-53802-4.00086-5.

Satake, K., and B. F. Atwater (2007), Long-term perspectives on giant earthquakes and tsunamis at subduction zones, *Annu. Rev. Earth Planet. Sci.*, *35*, 349–374, doi: 10.1146/annurev.earth.35.031306.140302.

Satake, K., and Y. Tanioka (1999), Sources of tsunami and tsunamigenic earthquakes in subduction zones, *Pure and Applied Geophysics*, *154*(3-4), 467–483, doi: 10.1007/s000240050240.

Scholl, D. W., S. H. Kirby, R. von Huene, H. Ryan, R. E. Wells, and E. L. Geist (2015), Great ($\geq$ M_w 8.0) megathrust earthquakes and the subduction of excess sediment and bathymetrically smooth seafloor, *Geosphere*, *11*(2), 236–265, doi: 10.1130/GES01079.1.

Seno, T. (2002), Tsunami earthquakes as transient phenomena, *Geophysical Research Letters*, *29*(10), doi: 10.1029/2002GL014868.

Sibuet, J.-C., C. Rangin, X. Le Pichon, S. Singh, A. Cattaneo, D. Graindorge, F. Klingelhoefer, J.-Y. Lin, J. Malod, T. Maury, et al. (2007), 26th December 2004 great Sumatra–Andaman earthquake: Co-seismic and post-seismic motions in northern Sumatra, *Earth and Planetary Science Letters*, *263*(1-2), 88–103, doi: 10.1016/j.epsl.2007.09.005.

Sieh, K., D. H. Natawidjaja, A. J. Meltzner, C.-C. Shen, H. Cheng, K.-S. Li, B. W. Suwargadi, J. Galetzka, B. Philibosian, and R. L. Edwards (2008), Earthquake supercycles inferred from sea-level changes recorded in the corals of west Sumatra, *Science*, *322*(5908), 1674–1678, doi: 10.1126/science.1163589.

Sladen, A., and J. Trevisan (2018), Shallow megathrust earthquake ruptures betrayed by their outer-trench aftershocks signature, *Earth and Planetary Science Letters*, *483*, 105–113, doi: 10.1016/j.epsl.2017.12.006.

Storchak, D. A., D. Di Giacomo, I. Bondár, E. R. Engdahl, J. Harris, W. H. Lee, A. Villaseñor, and P. Bormann (2013), Public release of the ISC–GEM global instrumental earthquake catalogue (1900–2009), *Seismological Research Letters*, *84*(5), 810–815, doi: 10.1785/0220130034.

Tanioka, Y., and T. Seno (2001), Sediment effect on tsunami generation of the 1896 Sanriku tsunami earthquake, *Geophysical Research Letters*, *28*(17), 3389–3392, doi: 10.1029/2001GL013149.

Tanioka, Y., L. Ruff, and K. Satake (1997), What controls the lateral variation of large earthquake occurrence along the Japan Trench?, *Island Arc*, *6*(3), 261–266, doi: 10.1111/j.1440-1738.1997.tb00176.x.

Titov, V., A. B. Rabinovich, H. O. Mofjeld, R. E. Thomson, and F. I. González (2005), The global reach of the 26 December 2004 Sumatra tsunami, *Science*, *309*(5743), 2045–2048, doi: 10.1126/science.1114576.

Van Rijsingen, E., S. Lallemand, M. Peyret, D. Arcay, A. Heuret, F. Funiciello, and F. Corbi (2018), How subduction interface roughness influences the occurrence of large interplate earthquakes, *Geochemistry, Geophysics, Geosystems*, *19*(8), 2342–2370, doi: 10.1029/2018GC007618.

Van Zelst, I. (2025), Data & scripts for 'Investigating global correlations between earthquake-generated tsunamis and subduction zone characteristics', doi: 10.5281/zenodo.7118751.

Van Zelst, I., L. Rannabauer, A.-A. Gabriel, and Y. van Dinther (2022), Earthquake rupture on multiple splay faults and its effect on tsunamis, *Journal of Geophysical Research: Solid Earth*, *127*(8), e2022JB024,300, doi: 10.1029/2022JB024300.

von Huene, R., J. J. Miller, D. Klaeschen, and P. Dartnell (2016), A possible source mechanism of the 1946 Unimak Alaska far-field tsunami: uplift of the mid-slope terrace above a splay fault zone, in *Global Tsunami Science: Past and Future, Volume I*, pp. 4189–4201, Springer, doi: 10.1007/s00024-016-1393-x.

Waldhauser, F., D. P. Schaff, T. Diehl, and E. R. Engdahl (2012), Splay faults imaged by fluid-driven aftershocks of the 2004 M_w 9.2 Sumatra-Andaman earthquake, *Geology*, *40*(3), 243–246, doi: 10.1130/G32420.1.

Wang, K., and S. L. Bilek (2011), Do subducting seamounts generate or stop large earthquakes?, *Geology*, *39*(9), 819–822, doi: 10.1130/G31856.1.

Wang, K., and S. L. Bilek (2014), Invited review paper: Fault creep caused by subduction of rough seafloor relief, *Tectonophysics*, *610*, 1–24, doi: 10.1016/j.tecto.2013.11.024.

Wang, Z., and J. Lin (2022), Role of fluids and seamount subduction in interplate coupling and the mechanism of the 2021 M_w 7.1 Fukushima-Oki earthquake, Japan, *Earth and Planetary Science Letters*, *584*, 117,439, doi: 10.1016/j.epsl.2022.117439.

Wendt, J., D. D. Oglesby, and E. L. Geist (2009), Tsunamis and splay fault dynamics, *Geophysical Research Letters*, *36*(15), doi: 10.1029/2009GL038295.

Ye, L., T. Lay, H. Kanamori, and L. Rivera (2016), Rupture characteristics of major and great (M_w 7.0) megathrust earthquakes from 1990 to 2015: 2. Depth dependence,

Journal of Geophysical Research: Solid Earth, *121*(2), 845–863, doi: 10.1002/2015JB012427.

Yokota, Y., T. Ishikawa, S.-i. Watanabe, T. Tashiro, and A. Asada (2016), Seafloor geodetic constraints on interplate coupling of the Nankai Trough megathrust zone, *Nature*, *534*(7607), 374, doi: 10.1038/nature17632.